Transport Problems

Volume 17 Issue 2

Problemy Transportu

WYDAWNICTWO POLITECHNIKI ŚLĄSKIEJ

GLIWICE 2022

SCIENTIFIC
JOURNAL

TRANSPORT PROBLEMS

Volume 17 Issue 2

PROBLEMY TRANSPORTU

Tom 17 Zeszyt 2

QUARTERLY

WYDAWNICTWO POLITECHNIKI ŚLĄSKIEJ
GLIWICE 2022

CONTENTS

Page

TRANSPORT PROBLEMS 2022 Volume 17 Issue 2
PROBLEMY TRANSPORTU DOI: 10.20858/tp.2022.17.2.02

Keywords: negative ions; car ionizer; mathematical modeling; comfort of car passengers

Mykola BILIAIEV[1], Oleksandr PSHINKO[2], Tetiana RUSAKOVA[3]*, Viktoriia BILIAIEVA[4], Aleksander SŁADKOWSKI[5]

MATHEMATICAL MODELING OF THE AEROION MODE IN A CAR

Summary. In this study, a mathematical method is proposed for calculating the concentration field of air ions of different polarities and dust levels in the passenger compartment, taking into account the geometry of the passenger compartment and seats, shelves, and other internal elements of the passenger compartment. The method also takes into account changes in the rate of the air flow ventilation, the location and number of ionizers, and sources of positive ions and dust, taking into account their different intensities and locations. On the basis of a numerical model for this method, software has been developed that allows users to carry out computational experiments without requiring much time for calculation. Based on the results, the optimal location of the ionizer in the passenger compartment of the car was determined to ensure comfortable conditions for the stay of passengers, which favorably affects their health. It has been found that the presence of two ionizers is optimal for creating comfort in the car with an ionization intensity of $Q_n = 0.47 \cdot 10^{10}$ ions/s located at the top of the car. If there is one ionizer located on the dashboard or at the top of the car with a higher ionization rate than $Q_n = 0.21 \cdot 10^{11}$ ions/s, it is not possible to simultaneously provide optimal ionization parameters for passengers in the front and rear seats of the car.

1. INTRODUCTION

Over the last few decades, much attention has been paid to the impact of polluted air on human health. Research [1-3] shows that polluted air adversely affects the respiratory, cardiovascular, nervous, and immune systems and is the main cause of increased morbidity among people living in cities. Due to intensive industrialization and urbanization, air pollution has become a serious global problem. There are many stationary and mobile sources of air pollution in cities. A short-term increase in PM2.5 levels increases the relative risk of acute cardiovascular disease by 1–3% [1]. An abundance of particles PM0.1 in the air is dangerous to human health. Usually, they enter the body through the lungs and move to almost all organs [2]. Compared to fine particles PM2.5, particles PM0.1 cause more severe lung inflammation and stay longer in the lungs. The toxicity of these particles increases as their size decreases. Such particles can be carriers of the severe acute respiratory syndrome virus caused by coronavirus [3].

[1] Ukrainian State University of Science and Technology; Lazaryan, 2, Dnipro, 49010, Ukraine; email: diit.hydro.eco@gmail.com; orcid.org/0000-0002-1531-7882
[2] Ukrainian State University of Science and Technology; Lazaryan, 2, Dnipro, 49010, Ukraine; email: Pshinko@mail.diit.edu.ua; orcid.org/0000-0002-1598-2970
[3] Oles Honchar Dnipro National University; Haharin av., 72, Dnipro, 49010, Ukraine; email: rusakovati1977@gmail.com; orcid.org/0000-0001-5526-3578
[4] Oles Honchar Dnipro National University; Haharin av., 72, Dnipro, 49010, Ukraine; email: vikabelyaeva604@gmail.com; orcid.org/0000-0003-2399-3124
[5] Silesian University of Technology; Krasiński 8, 40-019, Katowice, Poland; email: aleksander.sladkowski@polsl.pl; orcid.org/ 0000-0002-1041-4309
* Corresponding author. E-mail: rusakovati1977@gmail.com

People spend most of their time indoors, including up to 6% of their time in cars. A high level of concentration of harmful substances in the atmospheric air along roads is formed due to incomplete burning of fuel, which is determined by the type of engine, its service life, type of fuel, driving speed, as well as the low level of emission sources (car exhaust pipes) from the road surface. The untimely blocking of the supply ventilation leads to the entry of polluted air into the passenger compartment. However, the quantitative concentrations of particles in a car are significantly lower than their concentrations on the roads. The level of harmful substances concentration in the passenger compartment is also determined by the type of ventilation and the quality of the inlet and cabin filters [4]. Research shows that the highest levels of particle concentrations are observed at high speeds or under conditions of high traffic density (i.e., at low speeds) [5]. Since the inner volume of the passenger compartment is much smaller than the inner volume of any room, passengers are under the influence of a high concentration of fine particles and harmful substances, including those emitted from interior materials. The microenvironment in the passenger compartment influences the general physical and mental state of a person [6]. Therefore, the type and speed of ventilation, temperature, and emission features determine the microclimate inside a car [7].

Previous work [8] summarizes important data on air quality in passenger compartments, including chemical compounds that enter the cabin from various sources, and considers measurement techniques and control measures. Recently, various methods have been explored to solve indoor air purification problems: the generation of negative ions [9], photocatalysis of semiconducting material [10-11], ozone oxidation [12], filtration [13], the use of adsorbents [14], in-plasma (IPC) and post-plasma (PPC) catalysis for air purification [15], ultraviolet germicidal irradiation for air and surface disinfection [16]. Negative ion generators are beneficial, as they produce little noise, consume little power, do not require high maintenance costs, and provide a high level of purification [17-18].

The method of generating negative ions for air purification in rooms where people spend up to 80% of their time served as a prerequisite for its use to create a favorable microclimate in a passenger compartment. The car air ionizer is small and light, can be installed anywhere, and does not take up much space. A number of studies describe the mechanisms of formation, determining the concentration, and identifying negative ions [19]. Experimental works show that ionizers can be used for the highly efficient removal of dust particles, which are major air pollutants [20].

Since the level of ions in the passenger compartment is not satisfactory, staying a long time during the trip in a closed passenger compartment negatively affects both physical and mental state of a person. A low level of ions decreases energy and the ability to work; as a result, the person often feels drowsiness and fatigue. It is unacceptable to drive a car in this condition, as it can lead to various negative consequences, including traffic accidents.

The car air ionizer is designed to improve the quality of air in the passenger compartment by electrically charging the air particles, ionizing these particles, and removing pollutants. However, there are a number of problems regarding the effectiveness of car ionizers. For instance, it is necessary to choose the correct location for the ionizer in a car, as it is very important to ensure the required standard concentration of negative ions of about 3000-5000 ions/cm^3 near the respiratory organs of a person. The level of this concentration is influenced by various factors, including the performance of the ion emission source, the distribution of air flows in the passenger compartment, and the geometry of the compartment and internal components. The scientific rationale for using the different types of air ionizers that create a certain air ion regime in the passenger compartment can be quickly performed using the method of mathematical modeling. Carrying out physical experiments requires much time, special equipment, processing of measurement results, and obtaining final dependencies, which is not very convenient. Thus, the importance of creating effective mathematical models for predicting the air ion regime in passenger compartments is clear.

From a practical point of view, it is important to have physically substantiated mathematical models that allow predictions of the air ion regime in the passenger compartment that take into account the main physical factors that affect air ion dispersion and the interaction of ions in the air. In general, this kind of problem refers to the challenges of calculating the processes of mass transfer in the passenger compartment based on the pre-calculated air flow velocity field in the cabin.

The Navier-Stokes equations, supplemented by different turbulence models, are widely used to calculate the air flow velocity field in the passenger compartment, taking into account various kinds of obstacles. An example of such a calculation is shown in Fig. 1 [21]. However, the application of the Navier-Stokes equations requires the use of a fine grid, which requires computer time expenditures. This is not always convenient, especially if several calculations need to be computed. Therefore, from a practical point of view, it is important to have less complex mathematical models that require little computer time to calculate and allow the user to quickly analyze the distribution of the required parameter in the researched area.

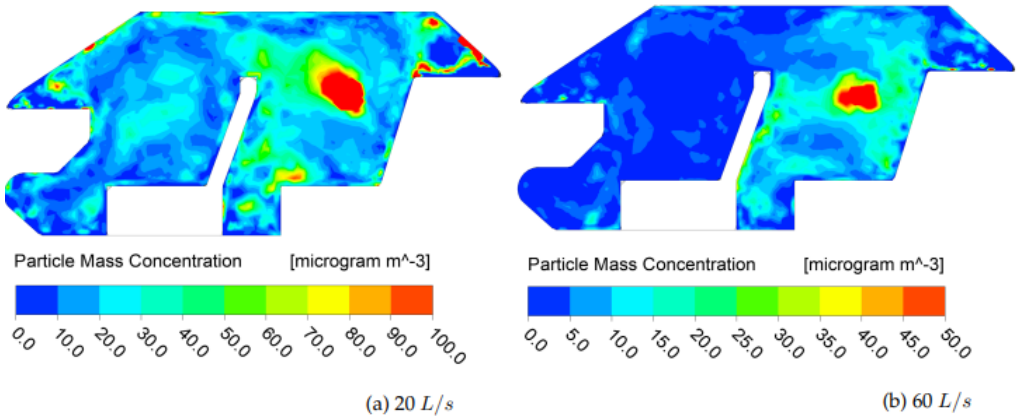

Fig. 1. The calculation of the concentration field of fine particles when smoking in a passenger compartment (the air flow velocity field was calculated based on the Navier-Stokes equations) [21]

The aim of this work is to develop a numerical method for predicting the air ion regime in the passenger compartment, thus making it possible to take into account the position of the ventilation holes, the air exchange mode, the mode of air ion emission, the presence of different obstacles, and possible dust pollution of the air.

2. STATEMENT OF THE RESEARCH PROBLEM

The passenger compartment of a LADA XRAY car is considered as an inner part of the area ABCDEFGHKL in the Oxy plane coordinate system. The cutting plane is drawn 0.4 m from the central section of the car. The geometrical dimensions are as follows: height = 122 cm; length = 330 cm; distance from the back of the front seat to the steering wheel = 85 cm; distance from the back of the rear seat to the back of the front seat = 90 cm (Fig. 2).

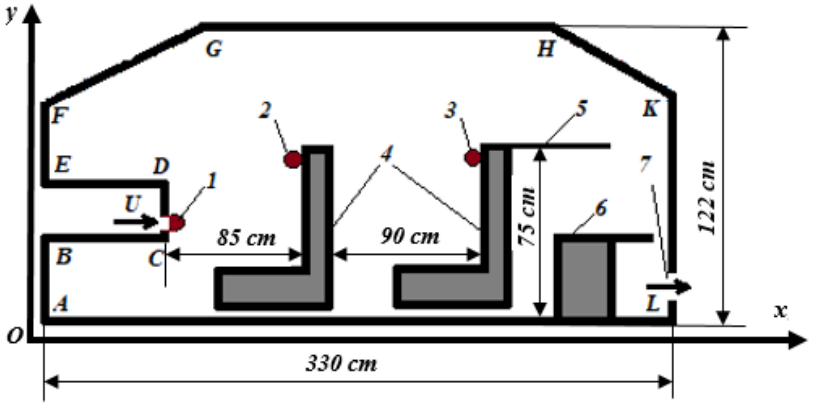

Fig. 2. Scheme of the calculation area of the passenger compartment: *1* – ionizer; *2,3* – sources of positive ions – human respiratory organs; *4* – seats; *5* – shelf behind the back seat; *6* – obstacles in the car trunk; *7* – exhaust opening; *U* – air speed in supply ventilation

The task is to study the concentration field of positive and negative air ions, dust, and the electric field in the car. A car ionizer is installed on the operation panel. It is known that the formation of the concentration field of air ions is influenced by a complex of physical factors, including air flow, diffusion, and the impact of an electric field. Moreover, ions of opposite charges interact with each other and with dust particles. A two-dimensional mass transfer equation is used to take these processes into account when modeling the dispersion of air ions in the passenger compartment. These equations are written for positive air ions, dust, and negative air ions. The modeling equations have the forms (1)–(3) [22].

Equation (1) is used to model the diffusion process of positive ions.

$$\frac{\partial C_p}{\partial t}+\frac{\partial (u+bE_{x)}C_p}{\partial x}+\frac{\partial (v+bE_y)C_p}{\partial y}=\frac{\partial}{\partial x}\left(\mu_x\frac{\partial C_p}{\partial x}\right)+\frac{\partial}{\partial y}\left(\mu_y\frac{\partial C_p}{\partial y}\right)-$$

$$-\alpha C_p C_n-\beta C_p C_d+\sum_{p_i=1}^{N_p} Q_{p_i}(t)\cdot\delta(x,y); \quad (1)$$

Equation (2) is used to model the dust transfer process.

$$\frac{\partial C_d}{\partial t}+\frac{\partial uC_d}{\partial x}+\frac{\partial vC_d}{\partial y}=\frac{\partial}{\partial x}\left(\mu_x\frac{\partial C_d}{\partial x}\right)+\frac{\partial}{\partial y}\left(\mu_y\frac{\partial C_d}{\partial y}\right)+\sum_{d_i=1}^{N_d} Q_{d_i}(t)\delta(x,y) \quad (2)$$

Equation (3) is used to model the diffusion process of negative ions.

$$\frac{\partial C_n}{\partial t}+\frac{\partial (u+bE_x)C_n}{\partial x}+\frac{\partial (v+bE_y)C_n}{\partial y}=\frac{\partial}{\partial x}\left(\mu_x\frac{\partial C_n}{\partial x}\right)+\frac{\partial}{\partial y}\left(\mu_y\frac{\partial C_n}{\partial y}\right)-$$

$$-\alpha C_n C_p-\beta C_n C_d+\sum_{n_i=1}^{N_n} Q_{n_i}(t)\cdot\delta(x,y). \quad (3)$$

The designations of the physical parameters in these equations are as follows: $C_p(x,y,t)$, $C_n(x,y,t)$ – concentration of positive, negative air ions, [ions/m^3]; $C_d(x,y,t)$ – concentration of dust particles respectively, [particles/m^3]; *u, v* – components of the air flow velocity vector, [m/s]; μ_x, μ_y – diffusion coefficients, [m^2/s]; *t* – time, [s]; α – recombination rate of ions that have different polarities, [m^3/(s·ions)]; β – recombination rate of ions with dust particles, [m^3/(s·ions)]; $Q_{p_i}(t)$, $Q_{n_i}(t)$ – emission intensity of positive, negative ions, [ions/(s·m^3)]; $Q_{d_i}(t)$ – dust emission intensity, [particles/(s·m^3)], $x_{p_i}, x_{n_i}, x_{d_i}, y_{p_i}, y_{n_i}, y_{d_i}$ – coordinates of emission sources of positive (negative) ions and dust, [m]; $\delta(x,y)$ – Dirac delta function; *b* – ion mobility coefficient [23], [m^2/(V·s)]; *E* – electric field strength, [V/m]. The *Oy* axis is directed vertically upwards; the *Ox* axis runs along the passenger compartment (Fig. 2).

The delta function is equal to zero everywhere except for the cells in which the *i-th* emission source is located. The emissions of positive ions, negative ions, and dust are modeled by point sources of a given intensity: $Q_{p_i}(t)$, $Q_{n_i}(t)$, $Q_{d_i}(t)$.

$\sum_{p_i=1}^{N_p} Q_{p_i}(t)\cdot\delta(x,y)$ – refers to the action of all sources of positive ions with their specific intensity taken into account, as well as the principle of superposition, where N_p – the number of emission sources (positive ions).

In a discrete form, the Dirac delta function is smeared over the area of the difference cell with the conservation of the total amount of matter (i.e., the intensity of the source is considered uniformly distributed over the cell). When the grid is thickened, we can find the value at the point.

For equations (1) – (3), the following boundary conditions are set:

1. At the boundary of the air flow entry into the passenger compartment, the concentration of negative and positive ions is set to zero ($C_p=0$, $C_n=0$).

2. At the boundary of the air flow entry into the passenger compartment, considering the dust concentration, the known value of the dust concentration at the entrance to the passenger compartment is set to $C_d = C_{d\,\text{entrance}}$.
3. At the location of the air ionizer, the intensity of their emission is set.
4. The emission of positive ions occurs as a person breathes. Since it is difficult in some cases to quickly determine the emission intensity of a certain parameter, such as positive ions, for models (1)–(3), the internal boundary condition of the first kind is realized (i.e., at the place where the source is located), and the concentration of this quantity is set, which is quite easy to measure. With this approach, the condition $C_p = C_{p\,\text{human}}$, where $C_{p\,\text{human}}$ is the known concentration of positive ions exhaled by a person, is set to the location of the passenger's head. The intensity of the emission of positive ions Q_{p_i} can also be set to the location of the human head.
5. On all solid walls, depending on the direction of the normal vector, the non-penetration condition must be satisfied, which requires that a change in the concentration along the normal vector to the surface must be equal to zero.
6. Diffusion is not taken into account at the boundary of the air flow outlet from the passenger compartment.
7. At the initial moment of time, it is assumed that the concentration of negative ions, positive ions, and dust is equal to zero. If necessary, it is possible to set any other value for the concentration of negative ions, positive ions, and dust. For example, this value can be determined based on experimental measurements or some background values.

When modeling the process for air ion dissemination, it is necessary to take into account the influence of the electric field. Since air ions have a charge, they generate an electric field with strength *E*. The following equation is used to model the electric field [22]:

$$\frac{\partial E_x}{\partial x} + \frac{\partial E_y}{\partial y} = \frac{q_e}{\varepsilon_0}, \tag{4}$$

where ε_0 – the dielectric constant; q_e – bulk charge density.

From equation (4), it is possible to pass to the scalar potential if such a dependence is taken into account:

$$E_x = -\frac{\partial \varphi}{\partial x}, \quad E_y = -\frac{\partial \varphi}{\partial y}. \tag{5}$$

Poisson's equation is obtained:

$$\frac{\partial^2 \varphi}{\partial x^2} + \frac{\partial^2 \varphi}{\partial y^2} = -\frac{q_e}{\varepsilon_0}, \tag{6}$$

where $q_e = -e\,C_p(x,y,t)$, $C_p(x,y,t)$ – positive ion concentration; φ – scalar potential; e – elementary charge. Based on this equation, the simulation of the electric field is performed.

The boundary condition for modeling equation (6) is the condition for the electrical insulation of surfaces in the cabin, $\frac{\partial \varphi}{\partial n_N} = 0$, where n_N – unit vector of the outward normal to the surface.

The movement of the air in the passenger compartment leads to the formation of an uneven air velocity field, which greatly complicates the theoretical solution when determining the ion concentration field in the cabin. There are seats inside the cabin that represent obstacles to the movement of air flow. Moreover, the position of the supply and exhaust holes also determine the aerodynamics of the air flows in the cabin. Therefore, before predicting the ion concentration in the cabin, based on the transfer equations (1) – (3) and (6), it is necessary to calculate the components of the air flow velocity vector *u, v* in the car cabin. A potential flow model is used to solve this aerodynamic problem [24]. It is necessary to integrate the Laplace equation for the velocity potential *P* to determine the values of the components of the air velocity vector in the passenger compartment:

$$\frac{\partial^2 P}{\partial x^2}+\frac{\partial^2 P}{\partial y^2}=0\,. \tag{7}$$

The corresponding boundary and initial conditions are set as shown in Fig. 2:

- At the location of the inlet (Fig. 2, designation *1*), where the flow enters the computational area, the Neumann boundary condition is set for the velocity potential $\frac{\partial P}{\partial x}=U$, where U – known air flow velocity.

- At the location of the exhaust hole, where the flow leaves the computational area, the Dirichlet boundary condition is set for the velocity potential $P=P_0+const$, where P_0 – some numeric constant equal to 100.

- The condition of non-penetration is set on solid impermeable walls, including the lower and upper boundaries of the area.

The components of the air flow velocity vector are calculated based on the dependencies [24]:

$$u=\frac{\partial P}{\partial x},\ v=\frac{\partial P}{\partial y} \tag{8}$$

3. NUMERICAL SIMULATION

For the numerical integration of the Laplace equation (7), an explicit method is used together with the splitting method. First, the Laplace equation (7) is reduced to an evolutionary type equation using the solution within a specific time. This approach was introduced by A.A. Samarsky and G.I. Marchuk when creating splitting methods. The resulting equation is geometrically split into two. At the next stage, these equations are approximated using the explicit difference scheme. The components of the air flow velocity vector are calculated based on the known values of the velocity potential [24].

The principle of integration of the transport equations (1) – (3) is considered based on the example of equation (1). At the differential level, this transport equation is split into three components, taking the following notation: $u+bE_x=u,\ v+bE_y=v$ for the convenience of splitting.

$$\frac{\partial C_p}{\partial t}+\frac{\partial uC_p}{\partial x}+\frac{\partial vC_p}{\partial y}=0\ , \tag{9}$$

$$\frac{\partial C_p}{\partial t}=\frac{\partial}{\partial x}\left(\mu_x\frac{\partial C_p}{\partial x}\right)+\frac{\partial}{\partial y}\left(\mu_y\frac{\partial C_p}{\partial y}\right), \tag{10}$$

$$\frac{\partial C_p}{\partial t}=\sum_{p_i=1}^{N_p} Q_{p_i}(t)\cdot\delta(x,y)\ . \tag{11}$$

In this splitting, equation (9) describes the process of impurity transfer under the action of the directed movement of the air flow. Equation (10) is the transfer under the action of diffusion, and Equation (11) is the change in the impurity concentration under the action of sources.

Next, the derivatives are approximated [24]. The time derivative is approximated by the divided «backwards» difference:

$$\frac{\partial C_p}{\partial t}\approx\frac{C_{p_{ij}}^{n+1}-C_{p_{ij}}^{n}}{\Delta t}\,.$$

For convective derivatives, the components of unidirectional transport are written as follows:

$$\frac{\partial uC_p}{\partial x}=\frac{\partial u^+C_p}{\partial x}+\frac{\partial u^-C_p}{\partial x};\qquad \frac{\partial vC_p}{\partial y}=\frac{\partial v^+C_p}{\partial y}+\frac{\partial v^-C_p}{\partial y}\,.$$

With the previous equations taken into account, the convective derivatives are approximated by «upstream divided» differences in the upper time layer:

$$\frac{\partial u^{+}C_p}{\partial x} \approx \frac{u^{+}_{i+1,j}C_p{}^{n+1}_{i,j} - u^{+}_{i,j}C_p{}^{n+1}_{i-1,j}}{\Delta x} = L^{+}_{x}C_p{}^{n+1}, \quad \frac{\partial u^{-}C_p}{\partial x} \approx \frac{u^{-}_{i+1,j}C_p{}^{n+1}_{i+1,j} - u^{-}_{i,j}C_p{}^{n+1}_{i,j}}{\Delta x} = L^{-}_{x}C_p{}^{n+1},$$

$$\frac{\partial v^{+}C_p}{\partial y} \approx \frac{v^{+}_{i,j+1}C_p{}^{n+1}_{i,j} - v^{+}_{i,l}C_p{}^{n+1}_{i,j-1}}{\Delta y} = L^{+}_{y}C_p{}^{n+1}, \quad \frac{\partial v^{-}C_p}{\partial y} \approx \frac{v^{-}_{i,j+1}C_p{}^{n+1}_{i,j+1} - v^{-}_{i,j}C_p{}^{n+1}_{i,j}}{\Delta y} = L^{-}_{y}C_p{}^{n+1}.$$

The velocity components u are determined based on the vertical sides of the difference cells, and the velocity components v are determined on the horizontal sides. The indices of these sides correspond to the indices of the cells located to the right or above the corresponding boundary.

At the next stage, the transport equation (9) is numerically solved using the following splitting scheme:

– At the first splitting step, the difference equation has the following form:

$$\frac{C_p{}^{k}_{i,j} - C_p{}^{n}_{i,j}}{\Delta t} + L^{+}{}_{x}C_p{}^{k} + L^{+}{}_{y}C_p{}^{k} = 0, \tag{12}$$

– At the second splitting step, the difference equation has the following form:

$$\frac{C_p{}^{n+1}_{i,j} - C_p{}^{k}_{i,j}}{\Delta t} + L^{-}{}_{x}C_p{}^{n+1} + L^{-}{}_{y}C_p{}^{n+1} = 0, \tag{13}$$

The unknown value of the concentration is found by an explicit scheme at each step of splitting (12) and (13).

For the numerical integration of the diffusion equation (10), a two-step difference splitting scheme is used (the method of total approximation) [24]:

$$\frac{C_p{}^{n+\frac{1}{2}}_{i,j} - C_p{}^{n}_{i,j}}{\Delta t} = \left[\mu_x \frac{-C_p{}^{n+\frac{1}{2}}_{i,j} + C_p{}^{n+\frac{1}{2}}_{i-1,j}}{\Delta x^2}\right] + \left[\mu_y \frac{-C_p{}^{n+\frac{1}{2}}_{i,j} + C_p{}^{n+\frac{1}{2}}_{i,j-1}}{\Delta y^2}\right], \tag{14}$$

$$\frac{C_p{}^{n+1}_{i,j} - C_p{}^{n+\frac{1}{2}}_{i,j}}{\Delta t} = \left[\mu_x \frac{C_p{}^{n+1}_{i+1,j} - C_p{}^{n+1}_{i,j}}{\Delta x^2}\right] + \left[\mu_y \frac{C_p{}^{n+1}_{i,j+1} + C_p{}^{n+1}_{i,j}}{\Delta y^2}\right], \tag{15}$$

The Euler method is used for the numerical integration of equation (11), and the calculated dependence has the following form:

$$C_p{}^{n+1}_{i,j} = C_p{}^{n}_{i,j} + \Delta t \cdot \sum_{p_i=1}^{N_p} Q_{p_i}(t) \cdot \delta(x,y) - \Delta t \alpha C_p C_n - \Delta t \beta C_p C_d \ . \tag{16}$$

For the numerical solution of the Poisson's equation (6), the following difference approximation is used:

$$\frac{\varphi_{i+1,j} - 2\varphi_{i,j} + \varphi_{i-1,j}}{\Delta x^2} + \frac{\varphi_{i,j+1} - 2\varphi_{i,j} + \varphi_{i,j-1}}{\Delta y^2} = -\frac{q_e}{\varepsilon_0}. \tag{17}$$

After calculating the scalar potential field $\varphi_{i,j}$, the components of the electric field strength are determined:

$$E_x = \frac{\varphi_{i+1,j} - \varphi_{i,j}}{\Delta x}, \ E_y = \frac{\varphi_{i,j+1} - \varphi_{i,j}}{\Delta y}. \tag{18}$$

The obtained value of E_x, E_y is used in the numerical solution of equations (1) and (3).

The program code «ION-2D» was created based on the constructed numerical model. FORTRAN was used for programming.

4. RESULTS OF THE PHYSICAL EXPERIMENT

When using the proposed method for assessing the air ion regime in the car, it is necessary to know the concentration of positive ions during human exhalation. Physical experiments were carried out from May 25–27, 2021, in Dnipro, Ukraine, from 10:00 a.m. until noon to obtain empirical evidence about the magnitude of such an emission. For the experiment, 16 people of different ages were selected, with four people in each age group: children, students, and university professors and elderly people. The measurements were taken in the passenger compartment of the LADA XRAY car, which did not move. The air temperature was 20–22 °C. The measurements were taken with each participant separately. All participants exhaled through the mouth so the concentration of positive ions and the air flow velocity could be measured during the exhalation 3 cm from the person's mouth (Fig. 3).

The area of the mouth was also measured; the average value was S=8.5 cm^2, the flow rate during exhalation was V=0.4 m/s for the age group of 40–45 years, and the flow rate (measured in m^3/s) and intensity of the emission of positive ions during exhalation were calculated as $I = V \cdot S \cdot C$ ions/s, where C ions/cm^3 is the concentration of positive ions during exhalation. The experiment to measure the concentration of air ions during human exhalation was carried out using an **Air Ion Tester**. The measurements of the average concentration of positive air ions during human exhalation for each age group are shown in Table 1.

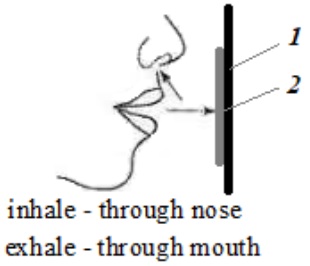

Fig. 3. Scheme of a physical experiment on measuring the concentration of positive ions: 1 – holder, 2 – device for measuring air ions

Table 1

Concentrations of positive air ions during human exhalations

Age (years)	Concentration of positive air ions (ions/cm^3)
8-9 (children)	166-176
18-19 (students)	232-349
40 (university professors)	277-329
78 (elderly people)	210-256

The data obtained on the basis of the physical experiment can be used when conducting computational experiments for the **quick** forecast of the air ion regime in the passenger compartment.

5. RESULTS OF COMPUTATIONAL EXPERIMENTS

The proposed numerical model was applied to solve the problem of forecasting the **ion mode** in the passenger compartment of a LADA XRAY car. The scheme of the computational domain (i.e., the interior of the car, in which the air-ion mode was modeled) is shown in Fig. 2.

The intake of negative ions into the car interior was carried out with the help of an ionizer with an intensity of negative ion emission $Q_n = 0.21 \cdot 10^{11}$ ions/s for the first scenario and $Q_n = 0.47 \cdot 10^{10}$ ions/s for the second scenario.

When modeling, it was assumed that additional dust sources are located on the floor, in front of the front and back seats, in the area where the passengers' feet are located (in Fig. 5, this area is indicated by the red line and marked D). The intensity of dust emission in front of the first seat is $Q_d = 0.0078$ mg/s, and the intensity of dust emission in front of the back seat is $Q_d = 0.0026$ mg/s.

The concentration of dust that enters the passenger compartment was considered equal to 0.025 mg/m^3 (i.e., the dust in the incoming air was not completely captured by the filter).

During the computational experiment, the following parameter values were utilized [21]: $\varepsilon_0 = 8.854 \cdot 10^{-12}$ K^2/(H·m^2) – medium permeability, $b = 2.4 \cdot 10^{-6}$ m^2/(V·s) – ion mobility; $e = 1.6 \cdot 10^{-19}$ K – elementary charge, $\alpha = 1.5 \cdot 10^{-12}$ (ions·m^3)/s, $\beta = 1 \cdot 10^{-12}$ (ions·m^3)/s.

During the calculations, it was assumed that the concentration of positive ions near the human head was 320 ions/cm^3. The dimensions of the computational domain – 3.3 m long, 1.22 m high; the speed of the air flow entering the passenger compartment – 0.43 m/s or 0.53 m/s. The turbulent diffusion coefficients in all directions were taken as equal to $\mu_x = 0.1 \cdot u(x,y)$, $\mu_y = 0.1 \cdot v(x,y)$, where *u(x,y), v(x,y)* are local air flow velocity components.

Fig. 4 shows the distribution of the positive ion concentration field in the passenger compartment, assuming an air flow rate of the supply ventilation of 0.43 m/s. The concentration value is presented as a percentage of the maximum in the calculation area. It can be seen from the figure that in the area where the respiratory organs of passengers are located, the maximum concentration of positive ions is observed.

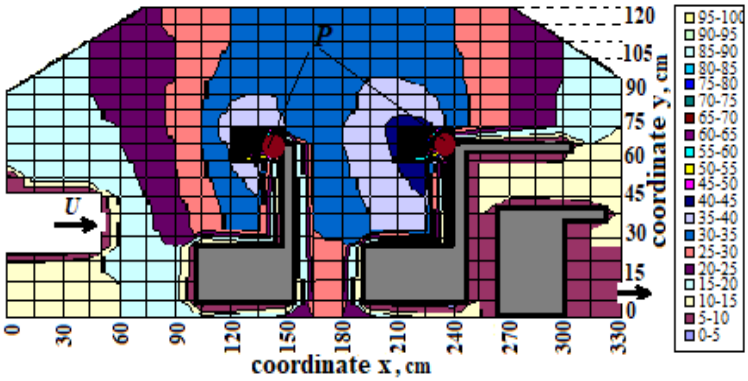

Fig. 4. The field of positive ion concentration in the car: *P* – sources of positive ions (human respiratory organs), $C_{p\,max}$=300 ions/cm^3

Fig. 5 shows the field of dust concentration distribution in the passenger compartment, which enters the supply ventilation, taking into account the influence of additional dust sources that arise in the area where the feet of passengers are located, as indicated in the figure by the red lines (indicated by *D*). It is clear that the maximum dust concentration is observed near the passenger seats, the area *A* (the front seat) – 80-50% and *B* (the back seat) – 60-40% within the maximum value of dust concentration 1.46 mg/m^3.

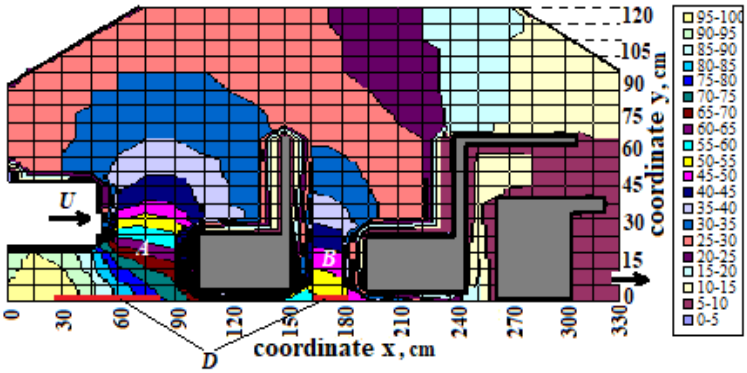

Fig. 5. The field of dust concentration in the passenger compartment, $C_{d\,max}$=1.46 mg/m^3

Fig. 6 shows graphs of the distribution of dust concentration (Fig. *6a*) and positive ion concentration (Fig. *6b*) at the seat-height level. As can be seen from Fig. *6a*, the maximum value of dust concentration is observed in front of the first seat and is C_{d1}=0.48 mg/m^3. Further, the

concentration decreases, as the seats act as an obstacle to the spread of dust. Thus, the concentration of dust at the head level of the second passenger is $C_{d\,2}$=0.37 mg/m^3. It should be noted that this value exceeds maximum allowable concentration at the level 0.16 mg/m^3 for PM2.5. At the end of the cabin, the dust concentration value is 0.16 mg/m^3, owing to the effect of exhaust ventilation. From Fig. *6b*, it can be seen that the peak concentration of positive ions is observed in the areas indicated in the figure by the letter *P*, which corresponds to the location of the sources of positive ions, namely the human respiratory organs. The minimum concentration of positive ions in the passenger compartment is C_p=48 ions/cm^3.

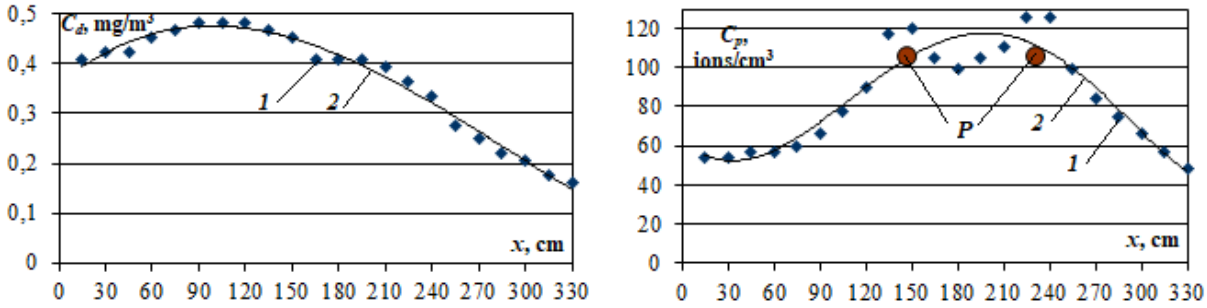

a *b*

Fig. 6. The distribution of dust and positive ion concentrations in the passenger compartment at the level of seat height: *a* – dust concentration; *b* – concentration of positive ions, *1* – results of numerical calculation; *2* – trend line in the form of polynomial dependence

When conducting a computational experiment for another air flow rate of supply ventilation equal to 0.53 m/s (i.e., with a 23% increase in speed), it was found that the maximum value of the dust concentration $C_{d\,\max}$ decreased by 5.5%, the local values of the dust concentration decreased by 7–9%, and the local values of the concentration of positive ions decreased by 5–6%. This indicates that an increase in the speed of the air flow in the passenger compartment slightly reduces the concentration of dust since there are various obstacles in the way of the air flow, which have a significant impact on the change in the structure of the flow.

A number of computational experiments were carried out, which made it possible to establish the most rational location of the ionizer in the passenger compartment without exceeding the maximum permissible negative ion concentration. Several scenarios were considered. In the first, the ionizer was located on the dashboard (Fig. 7, position *1*); in the second, it was located at the top of the cabin (Fig. 9, position *1*); in the third, two ionizers of lower power were utilized (Fig. 11, position *1*).

Fig. 7 shows the negative ion concentration field in the passenger compartment for the case where the ionizer is located on the dashboard. The maximum concentration was $C_{n\,\max}$=17090 ion/cm^3.

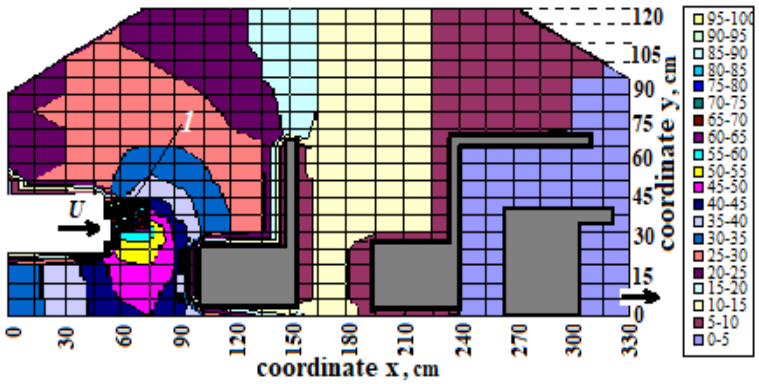

Fig. 7. Negative ion concentration field in the passenger compartment, $C_{n\,\max}$=17090 ion/cm^3, with one ionizer located on the dashboard – position *1*

Fig. 8 shows the distribution of negative ion concentration at the height of the seats. The concentration of negative ions (Fig. 8) at the head level of the first passenger is $C_{n\,1}$=4443 ions/cm^3,

which is the optimal value for a person. At the level of the second passenger's head, it is $C_{n\,2}$=1880 ions/cm^3, which is acceptable but not optimal. The maximum value of negative ion concentration of 4785 ions/cm^3 is reached at the level of the passengers' heads along the length of the cabin of 75–105 cm, which provides the first passenger with the optimal concentration.

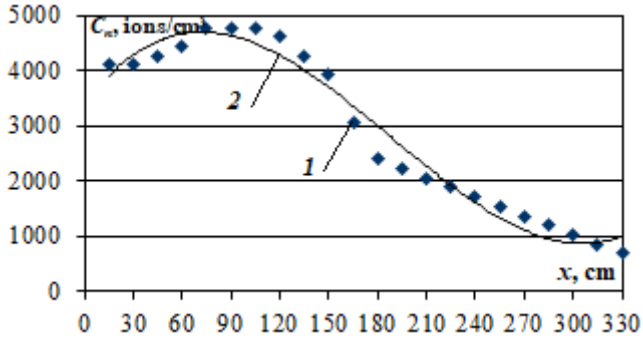

Fig. 8. The distribution of the concentration of negative ions in the passenger compartment at a seat height of y=75 cm in the presence of one ionizer located on the dashboard, *1* – results of numerical calculation; *2* – trend line in the form of polynomial dependence

However, the absence of additional sources of ionization and the presence of obstacles, namely the seats, causes the concentration of negative ions to decrease sharply at the level of the second passenger's head and further along the length of the cabin.

Thus, the location of the ionizer on the dashboard does not provide equable ionization of the passenger compartment. Therefore, a second variant of the ionizer location was considered (Fig. 9, position *1*) with the same ionization intensity at the top of the cabin, $Q_n = 0.21 \cdot 10^{11}$ ions/s. The concentration field changed (Fig. 9), and the maximum concentration value increased by 47% to $C_{n\,max}$=25080 ions/cm^3.

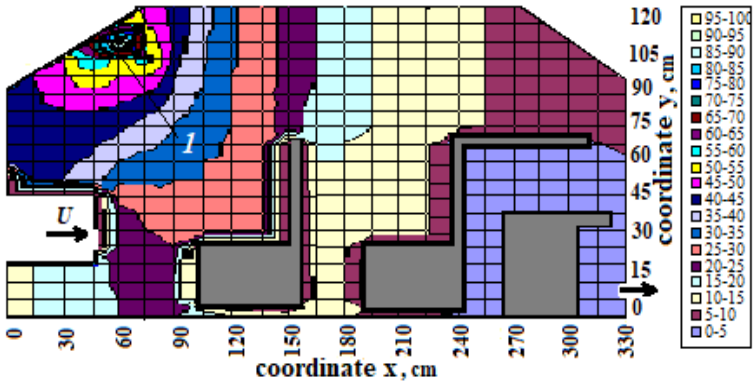

Fig. 9. The field of negative ion concentration in the passenger compartment, $C_{n\,max}$=25080 ions/cm^3, with one ionizer located at the top of the cabin – position *1*

Fig. 10 shows the distribution of negative ions at a seat height of y=75 cm with one ionizer located at the top of the cabin. The concentration of negative ions at the head level of the first passenger is $C_{n\,1}$=7273 ions/cm^3, which is beyond the optimal values for a person and is not favorable for their health. At the level of the second passenger's head, the concentration is $C_{n\,2}$=3261 ions/cm^3. This concentration promotes a person's comfort in the car. The maximum negative ion concentration of 10784 ions/cm^3 is reached at the level of the passengers' heads along the cabin length of 30–60 cm. However, the optimal ionization mode is provided for the second passenger due to the presence of seats, which serve as an obstacle for the air flow, which decreases the concentration near the head of the second passenger, creating optimal conditions while the first passenger remains outside the comfort zone. In further studies, the optimal location of the ionizer in the car was tested to ensure the comfort of both passengers.

Thus, a third variant of the location of two ionizers was considered (Fig. 11, position *1*) but with a lower ionization intensity, $Q_n = 0.47 \cdot 10^{10}$ ions/s. It can be seen that the concentration changed significantly, and the maximum concentration value decreased by more than two times to $C_{n\,max}$=7322 ions/cm^3.

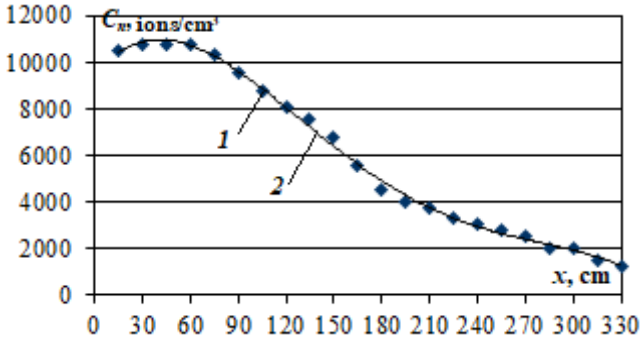

Fig. 10. The distribution of negative ion concentration in the passenger compartment at a seat height of y=75 cm, with one ionizer located at the top of the cabin, *1* – results of numerical calculation; *2* – trend line in the form of polynomial dependence

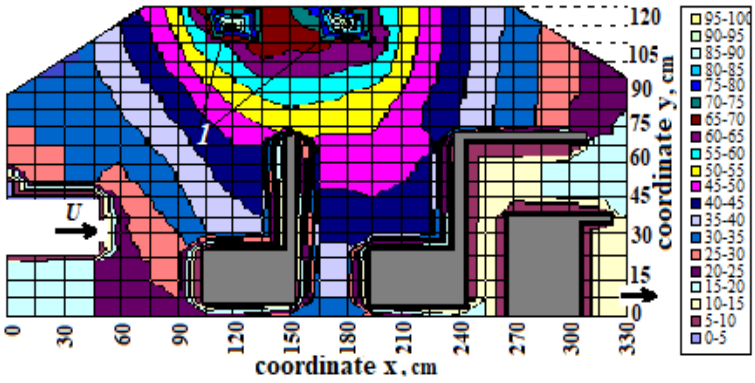

Fig. 11. The field of negative ion concentration in the passenger compartment, $C_{n\,max}$ =7322 ions/cm^3, in the presence of two ionizers located at the top of the cabin – position *1*

Fig. 12 shows the distribution of the negative ion concentration at the seat height of y=75 cm in the presence of two ionizers located at the top of the cabin. The maximum concentration of negative ions of 3954 ions/cm^3 is reached at the level of the passengers' heads along the cabin length of 165 cm.

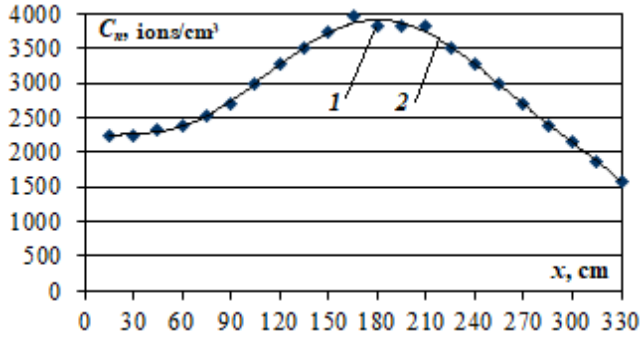

Fig. 12. The distribution of negative ion concentration in the passenger compartment at the seat height of y=75 cm, with two ionizers located at the top of the cabin, *1* – results of numerical calculation; *2* – trend line in the form of polynomial dependence

This concentration of negative ions is within the range of optimal values. The concentration of negative ions at the head level of the first passenger was $C_{n\,1}$=3358 ions/cm^3, and that at the level of

the second passenger's head was C_{n2}=3433 ions/cm^3, both of which are within the optimal range of concentration values for ensuring the comfort of both passengers in the car.

6. CONCLUSION

The mathematical method was developed to carry out calculations to determine the optimal location of the ionizer in the passenger compartment to ensure the comfort of passengers and favorably affect their overall health. The method takes into account the process of air ion scattering, the mutual influences of ions of different polarities and dust particles, and the influence of the electric field strength, which is formed by air ions.

The solution of the mass transfer equations and finding the air flow velocity field were performed by finite-difference methods using the method of splitting the mass transfer equation into three components: the equation of impurity transfer under the action of the directed movement of the air flow, the transfer equation within the diffusion, and the equation of impurity concentration change under the influence of sources. These equations were solved via two-step splitting using the upstream approximation, the total approximation, and the Euler method. The equation for finding the electric field strength was solved using a central-difference approximation of the derivatives.

This method takes into account the presence of obstacles—namely, seats—that affect the field of air flow velocity. The technique for carrying out numerical calculations using this method can take into account the geometry of the cabin and seats, shelves, and other internal elements, as well as the change in the rate of supply ventilation of the air flow. It is possible to set the following parameters when using this technique: the location of one or several ionizers, changes in the intensity of their ionization, the location and number of sources of positive ions, and the presence of several sources of dust while taking into account their different intensity and location.

The computational experiments revealed that the optimal setup for creating comfort in the car is to place two ionizers with an ionization intensity of $Q_n = 0.47 \cdot 10^{10}$ ions/s at the top of the car. With only one ionizer located on the dashboard or at the top of the car, the intensity of ionization is higher ($Q_n = 0.21 \cdot 10^{11}$ ions/s), and optimal parameters cannot simultaneously be provided for passengers in the front and back seats of the car. The time taken for one computational experiment was 15 seconds. The software implementation of this method can be used when carrying out serial calculations for preliminary estimation of the ionization level in the passenger compartment and the optimal location of one ionizer or possibly several ionizers to ensure a comfortable stay for passengers. Further research is planned to be carried out to aid the creation of a quick 3D model for calculating the process of ion and dust dispersion in the passenger compartment.

References

1. Rajagopalan, S. & Al-Kindi, S.G. & Brook, R.D. Air Pollution and Cardiovascular Disease: JACC State-of-the-Art Review. *Journal of the American College of Cardiology*. 2018. Vol. 72. No. 17. P. 2054-2070.
2. Schraufnagel, D.E. The health effects of ultrafine particles. *Experimental & Molecular Medicine*. 2020. Vol. 52. P. 311-317.
3. Zhu, C. & Maharajan, K. & Liu, K. & Zhanga, Y. Role of atmosphere particulate matter exposure in COVID-19 and other health risks in human*: A review Environmental Reserch.* 2021. Vol. 198. No. 111281.
4. Hudda, N. & Kostenidou, E. & Sioutas, C. & Delfino, R.J. & Fruin, S.A. Vehicle and driving characteristics that influence in-cabin particle number concentrations. *Environmental Science and Technol*ogy. 2011. Vol. 45(20). P. 8691-8697. Available at: http://dx.doi.org/10.1021/es202025m.
5. Bigazzi, A. & Figliozzi, M. Impacts of freeway traffic conditions on in-vehicle exposure to ultrafine particulate matter. *Environmental science & technology*. 2012. Vol. 60. P. 495-503.
6. Knibbs, L.D. & Cole-Hunter, T. & Morawska, L. A review of commuter exposure to ultrafine particles and its health effects. *Atmospheric Environment*. 2011. Vol. 45(16). P. 2611-2622.

7. Chen, X.K. & Feng, L.L. & Luo, H.L. & Cheng, H.M. Analyses on influencing factors of airborne VOCS pollution in taxi cabins. *Environmental Science and Pollution Research*. 2014. Vol. 21. P. 12868-12882.
8. Bin, Xu & Xiaokai, Chen & Jianyin, Xion Air quality inside motor vehicles' cabins: A review. *Indoor and Built Environment*. 2016. Vol. 27(4). P. 452-465.
9. Nadali, A. & Arfaeinia, H. & Asadgol, Z. & Fahiminia, M. Indoor and outdoor concentration of PM10, PM2. 5 and PM1 in residential building and evaluation of negative air ions (NAIs) in indoor PM removal. *Environmental Pollutants and Bioavailability*. 2020. Vol. 32. P. 47-55.
10. Chen, P. & Wang, H. & Liu, H. & Ni, Z. & Li, J. & Zhou, Y. & Dong, F. Directional electron delivery and enhanced reactants activation enable efficient photocatalytic air purification on amorphous carbon nitride co-functionalized with O/La. *Applied Catalysis B: Environmental*. 2019. Vol. 242. P. 19-30.
11. Qian, X. & Fuku, K. & Kuwahara, Y. & Kamegawa, T. & Mori, K. & Yamashita, H. Design and functionalization of photocatalytic systems within mesoporous silica. *ChemSusChem*. 2014. Vol. 7. P. 1528-1536.
12. Kwong, C.W. & Chao, C.Y. & Hui, K.S. & Wan, M.P. Removal of VOCS from indoor environment by ozonation over different porous materials. *Atmospheric Environment*. 2008. Vol. 42. P. 2300-2311.
13. Bekö, G. & Fadeyi, M.O. & Clausen, G. & Weschler, C.J. Sensory pollution from bag-type fiberglass ventilation filters: Conventional filter compared with filters containing various amounts of activated carbon. *Building and Environment*. 2009. Vol. 44. P. 2114-2120.
14. Monpezat, A. & Topin, S. & Deliere, L. & Farrusseng, D. & Coasne, B. Evaluation methods of adsorbents for air purification and gas separation at low concentration: Case studies on xenon and krypton. *Industrial Engineering Chemistry Research***.** 2019. Vol. 58. P. 4560-4571.
15. Van Durme, J. & Dewulf, J. & Sysmans, W. & Leys, C. & Van Langenhove, H. Efficient toluene abatement in indoor air by a plasma catalytic hybrid system. *Applied Catalysis B: Environmental.* 2007. Vol. 74. P. 161-169.
16. Kowalski, W. *Ultraviolet Germicidal Irradiation Handbook: UVGI for Air and Surface Disinfection*. Springer Science & Business Media: New York, NY, USA, 2010.
17. Shabani, B. & Hafttananian, M. & Khamani, S. & Ramiar, A. & Ranjbar, A.A. Poisoning of proton exchange membrane fuel cells by contaminants and impurities: Review of mechanisms, effects, and mitigation strategies. *Journal Power Sources*. 2019. Vol. 427. P. 21-48.
18. Guo, H. & Chen, J. & et al. A highly efficient triboelectric negative air ion generator. *Nature Sustainabilit*y. 2021. Vol. 4. P. 147-153.
19. Lin, H.-F. & Lin, J.-M. Generation and Determination of Negative Air Ions. *Journal of Analysis and Testing*. 2017. P. 1-6. DOI: http://dx.doi.org/10.1007/s41664-017-0007-7.
20. Jiang, S.-Y. & Ma, A. & Ramachandran, S. Negative air ions and their effects on human health and air quality improvement. *International Journal of Molecular Sciences*. 2018. Vol. 19(10). No. 2966. P. 1-19.
21. Ljung, S. *CFD simulation of particle matter inside an automotive car and the purification efficiency of cabin air purifier. Appendix B. Particle Fate*. 2019. 50 p.
22. Беляев, Н.Н. & Цыганкова, С.Г. *Моделирование аэроионного режима в помещении при искусственной ионизации воздуха.* Днепропетровск: ПГАСА, 2016. 109 p. [In Ukrainian: Belyaev, N.N. & Tsygankova, S.G. *Simulation of the air-ion regime in a room with artificial air ionization*. Dnepropetrovsk: PGASA].
23. Fletcher, L.A. & Noakes, C.J. & Sleigh, P.A. & Beggs, C.B. & Shepherd, S.J. Air ion behavior in ventilated rooms. *Indoor and Built Environment*. 2008. Vol. 17(2). P. 173-182. DOI: http://dx.doi.org/10.1177/1420326X08089622.
24. Biliaiev, M. & et al. Computing model for simulation of the pollution dispersion near the road with solid barriers. *Transport Problems*. 2021. Vol. 16. No. 2. P. 73-86.

Received 02.10.2020; accepted in revised form 16.05.2022